Enigmatic tsunami waves amplified by repetitive source events in the southwest of Torishima Island, Japan

Osamu Sandanbata[1][†], Kenji Satake[1], Shunsuke Takemura[1], Shingo Watada[1], and Takuto Maeda[2]

[1]Earthquake Research Institute, The University of Tokyo, Tokyo, Japan.

[2]Graduate School of Science and Technology, Hirosaki University, Aomori, Japan.

Corresponding author: Osamu Sandanbata (osm3@eri.u-tokyo.ac.jp)

Key Points

- On 9 October 2023 (JST), enigmatic tsunamis up to ~60 cm were recorded along broad Japanese coasts without large earthquakes.

- Analysis of stacked bottom-pressure data shows >10 repetitive events for ~1.5 hr intermittently produced tsunamis with T-phase excitation.

- Larger events in later sequence occurred with intervals similar to the wave period, amplifying the tsunami waves in later phase.

Abstract

On 9 October 2023 (JST), mysterious tsunamis with a maximum wave height of 60 cm were observed in Izu Islands and southwestern Japan, although only seismic events of body-wave magnitudes m_b 4–5 have been documented in the southwest of Torishima Island. To investigate the source process, we analyze tsunami waveforms recorded by an array network of ocean-bottom pressure gauges. A stacked waveform of 16 records suggests recurrent arrivals of multiple wave trains. Deconvolution of the stacked waveform by a tsunami waveform from the first event revealed over 10 source events that intermittently generated tsunamis for ~1.5 hours. The temporal history of this sequence corresponds to the origin times of T-phases estimated by an ocean-bottom seismometer, and the m_b 4–5 seismic swarm, implying a common origin. Larger events later in the sequence occurred at intervals comparable to the tsunami wave period, causing amplification of later phases of the tsunami waves.

Plain Language Summary

On 9 October 2023 (JST), mysterious tsunamis hit Izu Islands and southwestern Japan, reaching up to 60 cm in height, although only small-to-moderate seismic events were reported in the region. To resolve how the mysterious tsunami waves were generated, we analyze the waves recorded by a tsunami observation network off the southwestern coast of Japan. We find that the tsunami waves were intermittently produced by repetitive source events for approximately 1.5 hours, and the wave amplification happened because the event interval time matched the wave period. These abnormal submarine events excited significant acoustic oceanic waves, as well as large tsunamis, which would provide valuable information to further study what took place in the ocean.

41

1 Introduction

On 9 October 2023 (JST, +09UTC), enigmatic tsunamis were observed along coasts in broad region from south to west of Japan. The tsunami heights, measured from zero to crest, were 30–60 cm in Izu Islands (Yaene, Tsubota, and Kozushima) and the Kanto region (Mera), and 30–40 cm tsunamis were recorded even in distant stations (Tosa-shimizu and Nakanoshima) (Japan Meteorological Agency, 2023) (Figure 1a). Because no significant earthquake was observed and no offshore tsunami observation system is deployed off Izu-Bonin Islands, the tsunami forecasting system did not work well; it was only after the tsunami was clearly recorded by a tsunami-meter at Yaene on Hachijojima Island that the tsunami advisory was issued by Japane Meterorological Agency (JMA).

From 3:58 to 6:21 (JST) on the day, 13 small-to-intermediate seismic events of body-wave magnitudes m_b 4.3–5.4 in the oceanic region approximately 80 km southwest of Torishima Island were reported in the earthquake catalog of U. S. Geological Survey (USGS; Figure 1c); here, these seismic events are labelled as *Se01–13* (Table S1). The amplitudes of the observed tsunamis were by far larger than those expected from the seismic magnitudes; the tsunami magnitude based on the maximum amplitude information reported by JMA is estimated as M_t 8.0 (Abe, 1981). This fact suggests the atypical source mechanism of the tsunamis. For such tsunamis without large earthquakes, various types of source mechanism have been proposed: for example, slow-ruptured tsunami earthquakes along subduction zones (e.g., the 1896 Sanriku earthquake, the 1946 Aleutian earthquake) (Kanamori, 1972; Tanioka & Satake, 1996), oceanic volcanic processes (e.g., the 2018 Anak Krakatau eruption, the 2022 Hunga Tonga–Hunga Haʻapai eruption) (Kubota et al., 2022; Mulia et al., 2020; Paris, 2015), or submarine/coastal

64   landslides or mass failures (e.g., the 1998 Papua New Guinea tsunami) (Synolakis et al., 2002;

65   Tappin et al., 1999).

66   In this study, we investigate the source process of the enigmatic tsunami waves using

67   tsunami waveform data recorded by an array network of ocean-bottom-pressure (OBP) gauges

68   off the southwestern coast of Japan. We first apply a waveform stacking technique to the

69   multiple tsunami waveforms, and then estimate the temporal history of the tsunami generation

70   based on analysis of the stacked data. Consequently, we propose their peculiar tsunami origin by

71   repetitive source events that took place intermittently for ~1.5 hours.

72   **2 Data**

73   The tsunami waves were recorded by the dense OBP gauges of Dense Oceanfloor

74   Network system for Earthquakes and Tsunamis (DONET) off the southwestern coast of Japan

75   (Figure 1b) (National Research Institute for Earth Science and Disaster Resilience, 2019). In

76   Figure 2a, we show the OBP data after removing the tidal component, demonstrating repetitive

77   strong high-frequency signals with dominant frequencies of higher than 1 Hz approximately

78   from 4:00 to 6:30 (see Figure S1). These high-frequency signals are confirmed to be T-phases,

79   seismic waves converted from oceanic acoustic waves (Okal, 2008), based on their arrival times

80   explained by a typical T-phase speed of 1.5 km/s from the origin times and locations of the

81   seismic events. Following the T-phase signals, tsunami waves with longer periods were

82   recorded, as shown evidently in the band-pass (0.00125–0.02 Hz/50–800 s) filtered records

83   (Figure 2b). Smaller oscillations start around 5:40, leading to the largest amplitudes of ~20 mm

84   after ~7:00. Thus, the tsunami oscillations continued for hours with late arrivals of large

85   amplitude waves.

86   To capture the features, a tsunami waveform stacking technique is applied to 16 OBP

87   records of DONET1, listed in Table S2. By assuming a point source at the epicenter location

88   (140.026°E, 29.787°N) of the m_b 5.4 seismic event (Se12), the largest event among the swarm,

89   the tsunami travel times to the OBP gauges are computed by a shallow-water-wave tsunami

90   model of the Geoware TTT Software (Figure S2). The band-pass filtered waveform at each OBP

91   is shifted in such a way that the arrival times are aligned with that at the earliest-arrival station

92   (KMC21). We then stack the time-shifted waveforms and take the amplitude average and

93   standard deviation.

94   As shown in Figures 3a and 3b, all the OBP waveforms used here show similar shapes;

95   thereby, the waveform stacking yields clear tsunami waveforms only with small standard

96   deviations. The tsunami waves initiate at ~120 min (~5:30) and reach the maximum amplitude at

97   ~220 min (~7:10).

98   For further investigation, we apply the wavelet analysis to the stacked waveform (Figure

99   3c). The obtained scalogram shows that the tsunami signals are composed of multiple bends of

100   dispersive amplitude peaks with early arrival of lower-frequency amplitude followed by higher-

101   frequency amplitude (red arrows and a curly bracket in Figure 3c). This character with multiple

102   bands is quite different from a tsunami event originating from a single volcanic earthquake at

103   Sumisu Caldera, which shows only a single band (Figures S3; see the caption for details).

104   Therefore, we speculate that multiple tsunami wave trains, each with a strongly dispersive

105   character, recurrently arrived at the OBP gauges.

106 **3 Estimation of source time function**

107 We investigate the temporal history of the tsunami generation process by using the

108 iterative deconvolution method (Kikuchi & Kanamori, 1982), widely applied for earthquake

109 source studies.

110 We hypothesize that multiple impulsive source events took place at the same location but

111 at different timings, and that each single event produced tsunami waveforms with the same

112 shapes and different amplitudes. Under this hypothesis, the stacked OBP tsunami waveform is

113 the convolution of the temporal history of multiple impulsive events, or the *tsunami source time*

114 *function* (STF), and the tsunami waveform produced by a single event, or the *Green's function*.

115 Denoting the stacked tsunami waveform as $d(t)$ and the Green's function as $w(t)$, the

116 convolution can be expressed, as follows:

117 $$d(t) = \sum_i m_i w(t - t_i), \qquad (1)$$

118 where m_i and t_i represent the source amplitude and the timing of the i-th source event (note that

119 i represents the iteration time, not the order in time, as explained below).

120 The Green's function is extracted from the stacked tsunami waveform data. We first

121 confirm that the theoretical arrival times of the tsunamis caused by the two early earthquakes,

122 Se02 and Se03 (Table S1), agree well with the timings when the tsunami signal initiates (~5:40)

123 and when the amplitude increases (~6:00), respectively (arrows in Figure 4a). We assume that

124 the signal between the two tsunami arrival times represent the tsunami waveform due to Se02,

125 and construct the Green's function with an initial zero-amplitude data for the length of the

126 theoretical tsunami travel time, followed by the stacked waveform in the time window (with

127 tapering on the 5% edges) (green line in Figure 4a). m_i in Equation (1) now represents the

128 relative source amplitude of the *i*-th source event to that of Se02, and we impose $m_i \geq 0$ under

129 our hypothesis of multiple similar events.

130   Using the Green's function, we deconvolve the stacked tsunami waveform (Figure 4a) to

131 estimate the tsunami STF, following Kikuchi and Kanamori (1982). Denoting the stacked

132 tsunami waveform as $x(t)$, we first take a single event and determine m_1 and t_1 by minimizing

133 the error defined as:

134      $$\Delta_1 = \int_0^T [x(t) - m_1 w(t - t_1)]^2 dt, \quad (2)$$

135 where T is the length of the stacked waveform, and obtain the residual waveform:

136      $$x^{(1)}(t) = x(t) - m_1 w(t - t_1). \quad (3)$$

137 In the next iteration, we determine m_2 and t_2 by minimizing the error Δ_2 for the residual

138 waveform $x^{(1)}(t)$, and obtain the residual waveform:

139      $$x^{(2)}(t) = x^{(1)}(t) - m_2 w(t - t_2). \quad (4)$$

140 We iteratively repeat the procedure above until the approximation error changes by less than 2%

141 by an iteration $((\Delta_{i-1} - \Delta_i)/\Delta_{i-1} < 0.02)$. The approximation accuracy is quantified by the

142 normalized approximation error by

143      $$\Delta_i/\Delta_0 = \int_0^T [x^i(t)]^2 dt / \int_0^T [x(t)]^2 dt. \quad (5)$$

144 Thus, we determine the relative source amplitudes of m_i at the timings of t_i $(i = 1, \dots N)$.

145   We find that, in the iterative deconvolution process, the source amplitudes determined in

146 earlier iterations tend to be larger, because the original observed waveform is fit mainly by

147 earlier-determined events, and later events are fit to the residual waveforms (Kikuchi &

148 Kanamori, 1982). As seen in the iterative deconvolution results (Figure S4), a source event at

149   6:17, determined in the first iteration, has a very large source amplitude. To examine how

150   reliable the results are, we re-determine the source amplitudes by an additional least-squares

151   method. While fixing the source event times t_i, we re-estimate the source amplitude m_i' by

152   minimizing the following error by the non-negative least-squares method:

153    $\qquad x(t) - \sum_{i=1}^{N} m_i' w(t - t_i).$ (6)

154   Thus, we obtain the tsunami STF, represented by the relative source amplitude m_i' at the source

155   times of t_i. The tsunami waveform is modeled with Equation (1), where m_i is replaced by m_i'.

156   The additional least-squares method improves the amplitude balance of several source events

157   close in time, determines the amplitude of an event as zero, which we remove from the event list;

158   then, the normalized approximation error is reduced significantly from 0.174 to 0.118 (compare

159   Figure S4 with Figure 4).

160   **4 Results**

161   We obtain the tsunami STF composed of 23 single-source events that span from 4:54 to

162   7:02, labeled as *Ts01–23* (Figure 4 and Table S3). The fit between the stacked waveform and the

163   convolved waveform is remarkably good (Figure 4b). This suggests that repetitive tsunami

164   source events took place with a similar mechanism at similar locations, intermittently producing

165   similar tsunami waveforms.

166   Major source events are estimated from 4:54 (Ts01) to 6:34 (Ts18) for over 1.5 hours

167   (Figure 4c). Some of these events are close to each other with a time difference of only <~100 s

168   (Ts06–07, and Ts09–10). These may be separately deconvolved from a single event due to

169   unmodeled later phases of prior events (e.g., coastal reflected waves), not included in the Green's

170   function. Given the limitation, we exclude Ts06 and Ts10, a smaller event among each pair, from

171   major events. Later events, Ts19–23, may be also artifacts arising for the same reason. Then, the

172   sequence of the major events gradually increases the amplitude from 1.0 to 6.5 and reduces the

173   interval time approximately from 1,200 s to 250 s.

174   Most of the later major events with larger amplitudes (e.g., Ts11–15) occur with interval

175   of 200–300 s (Figure 4c, and Table S3), which are comparable to the dominant period of the

176   observed tsunami waveforms (Figure 3c). Figure 5a shows tsunami waveforms from Ts11–15,

177   each of which has a non-negligible amplitude of ~10 mm, less than half of the amplitude of the

178   stacked largest waves between 7:00 and 7:20. Yet, their waveform phases match with each other,

179   and thereby the superposition of the tsunami waveforms doubles the wave amplitude and

180   reproduces the largest waves (Figure 5b). Therefore, the late arrivals of large tsunami waves can

181   be attributed to the later large events with interval times similar to the characteristic period of the

182   tsunami waves.

183   The major source events in the tsunami STF correlate well with the swarm of seismic

184   events. In Figure 4d, we compare the tsunami STF with the sequence of seismic events Se01–13,

185   reported in the USGS catalog (Table S1). Each of the seismic events of Se02–13, excluding

186   Se01, nearly coincides with one of the major tsunami source events, Ts01–15. The overall trend

187   in event size is also similar to that of the tsunami STF.

188   As shown in Figure 2a, strong T-phase signals were repetitively recorded. We investigate

189   their origins by analyzing the up-down component of a broadband seismometer at KMB06

190   (Figure 1b); we first apply the band-pass (1–6Hz) filter, convert the waveform into envelope by

191   the Hilbert transform and the moving average with a 5-s window, and identify T-phase signals

192   with a maximum amplitude larger than an empirical threshold of 2.0×10^3 nm/s. The origin times

193   of the T-phase signals are determined by shifting the maximum amplitude time backward by the

194   travel time from the Se12 location to KMB06 (5.48 min). As results, we detect 14 T-phase

195   events, labeled as *Tp01–14*, as listed in Table S4. The temporal history of the T-phase events,

196   except for Tp01, agrees with the tsunami STF, as well as the seismic event swarm (Figure 4d), in

197   terms of the origin times and the overall trend in size.

198   **5 Discussion & Conclusions**

199   Table S5 summarizes 14 source events (labeled as *EV01–14*), which have similar origin

200   times based on data of tsunami waves, seismic waves, and T-phases. EV01 at ~4:00 and EV11 at

201   ~6:09 are missing in the tsunami STF and in the USGS catalog, respectively, whereas all the

202   other events are commonly detected as tsunami and seismic wave, and T-phase sources. Note

203   that the envelope shape of the T-phase signal from EV01, or Tp01, indicates its longer source

204   duration than those of the others (Figure 4d and Table S4); this may explain why EV01 did not

205   generate noticeable tsunami waves, since a long-duration tsunami generation process with a

206   small source area cannot displace the water height efficiently (Saito & Furumura, 2009).

207   We have revealed that the repetitive events excited strong acoustic (*P*) waves that are

208   converted to T-phases and generated large tsunami waves, but radiated only minor seismic waves

209   equivalent to m_b 4–5. Although the mechanism of the repetitive events remains to be solved, the

210   coincidental excitation of strong T-phases and large tsunamis suggests a very shallow source

211   depth in the crust or just on the seafloor. T-phase data may a constrain the water depth where the

212   events took place, because T-phases are more effectively excited in a water depth of ~1,000 m, a

213   range of the so-called SOFAR channel (Okal, 2008). On the other hand, the tsunamigenesis

214   requires a large volume of displaced seawater by such as seafloor deformation or mass

215   movement on the seafloor. Several possible candidates that satisfy both conditions remain.

216   Volcanic processes in the ocean, ranging from eruptions (Purkis et al., 2023; Yamasato et al.,

217   1993), flank failures (Grilli et al., 2019), intra-caldera faulting (Sandanbata et al., 2023), and

218   caldera collapse (Maeno et al., 2006) may explain these characters. Repetitive T-phase events

219   following a non-double-couple earthquake (M_w 5.7) in 1996 near Sumisu Caldera (Figure 1c),

220   which caused a large tsunami, were attributed to submarine volcanic phenomena (Sugioka et al.,

221   2000). Submarine landslides or mass failures can be also possible, as T-phases were recorded

222   around the timing of the 1998 Papua New Guinea tsunami (Okal, 2003). Faulting events cannot

223   be excluded from candidates, but in this case, the source depth must be very shallow in the crust,

224   given the low seismic excitation (Fukao et al., 2018). A compilation of different datasets of

225   tsunamis, seismic waves, and T-phases would be the key to determine the mechanism. More

226   direct information may be obtained by ship-borne surveys of the bathymetry change in the source

227   region.

228   The character of the repetitive events is informative to know how the series of

229   phenomena proceeded. As seen in Figures 5c and 5d, the source event number increases

230   exponentially with time; in other words, the inter-event interval of the events exponentially

231   decreases. Geological phenomena with similar characteristics of decreasing inter-event interval

232   were previously reported as precursors for landslide events (Yamada et al., 2016), collapse

233   events of volcanic calderas (Michon et al., 2009), and for fault slip in a critical state in tectonic

234   environment (Igarashi, 2000).

235   The 9 October 2023 tsunami followed a previous seismic swarm mainly from 2 to 6

236   October, including two M_w>6 earthquakes in the source region (Figure 1c). The relationship

237   between the tsunami event and the preceding swarm is unclear, but we note that some

238   earthquakes on 5 October radiated much stronger seismic waves than the 9 October sequence,

239   although signals in the frequency range of 1–4.99 Hz, where T-phase are dominant, are larger for

240   the latter (compare Figures S1 and S5), indicating a big difference in their source mechanisms or

241   source depths. One possible hypothesis for the link is that the seismic swarm was related to the

242   movement of magma in the crust, leading to another phase of volcanic process, such as

243   underwater eruptions, volcanic deformation, or flank collapses. Another is that ground shaking

244   due to the preceding swarm destabilized parts of sloped bathymetry in this region, leading to

245   submarine mass failures a few days later.

246   The enigmatic tsunami event on 9 October 2023 sheds light on the difficulty in

247   forecasting the types of tsunamis not accompanying any significant earthquake in the Izu-Bonin

248   region, where no offshore tsunami observation system is deployed. The coincidence of strong T-

249   phases with tsunami generation may help us to estimate the tsunami potential in advance, as has

250   been long suggested (Ewing et al., 1950; Matsumoto et al., 2016). However, the Izu-Bonin

251   region hosts a number of volcano islands, submarine volcanoes, and active back-arc rift systems

252   (Kodaira et al., 2007), suggesting various types of potential tsunami hazards. Previously, another

253   series of peculiar tsunamis have recurrently taken place, almost every 10 years, due to M_w 5.4–

254   5.8 volcanic earthquakes at Sumisu Caldera, ~100 km north of Torishima Island (Figure 1c)

255   (Kanamori et al., 1993; Satake & Kanamori, 1991); a submarine trapdoor faulting in the caldera

256   was recently proposed for the series (Sandanbata et al., 2022). In another case, an M_w 6.4 normal

257   faulting earthquake on 24 October 2006 in a region between Sofugan and Nichiyo Seamont

258   (Figure 1c) also caused about 10-cm tsunamis (Japan Meteorological Agency, 2023). In this

259   context, there is an urgent need to improve preparedness for potential tsunami occurrences in the
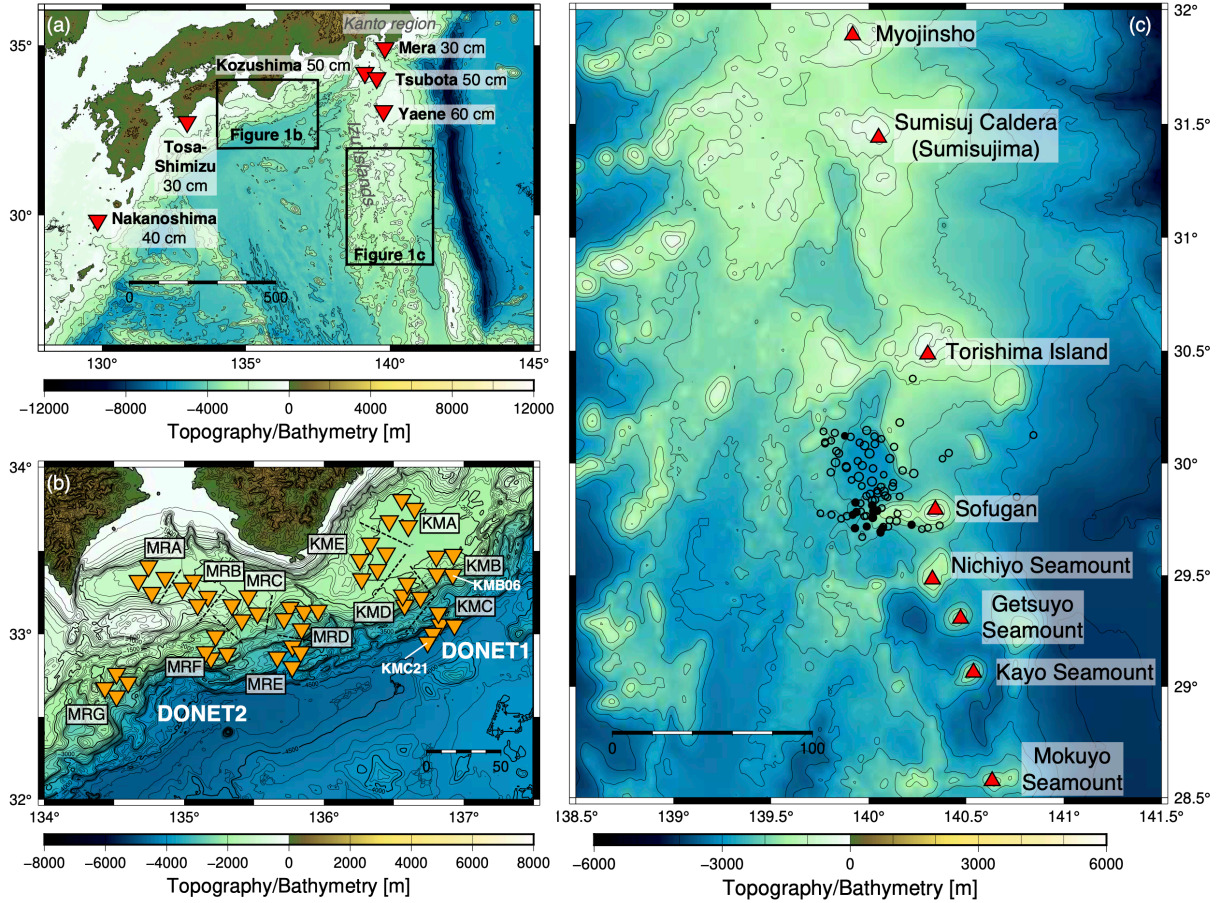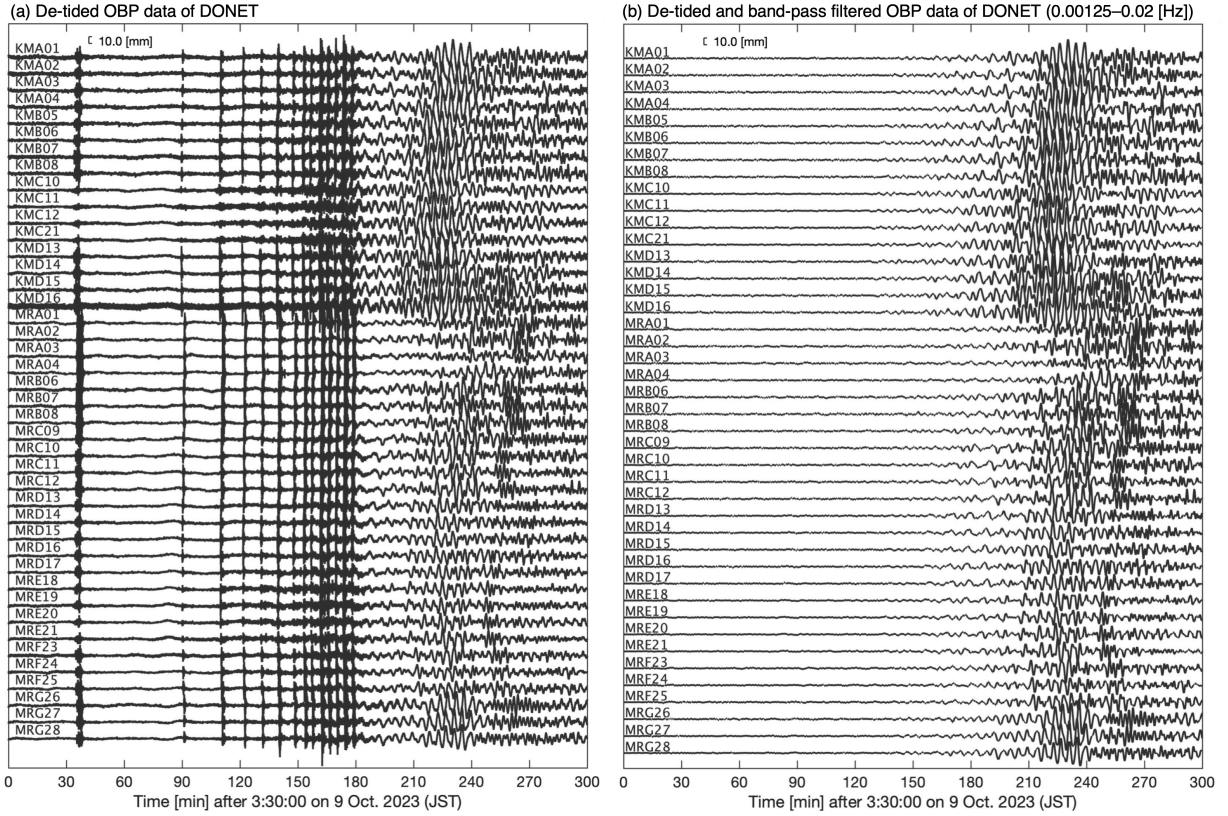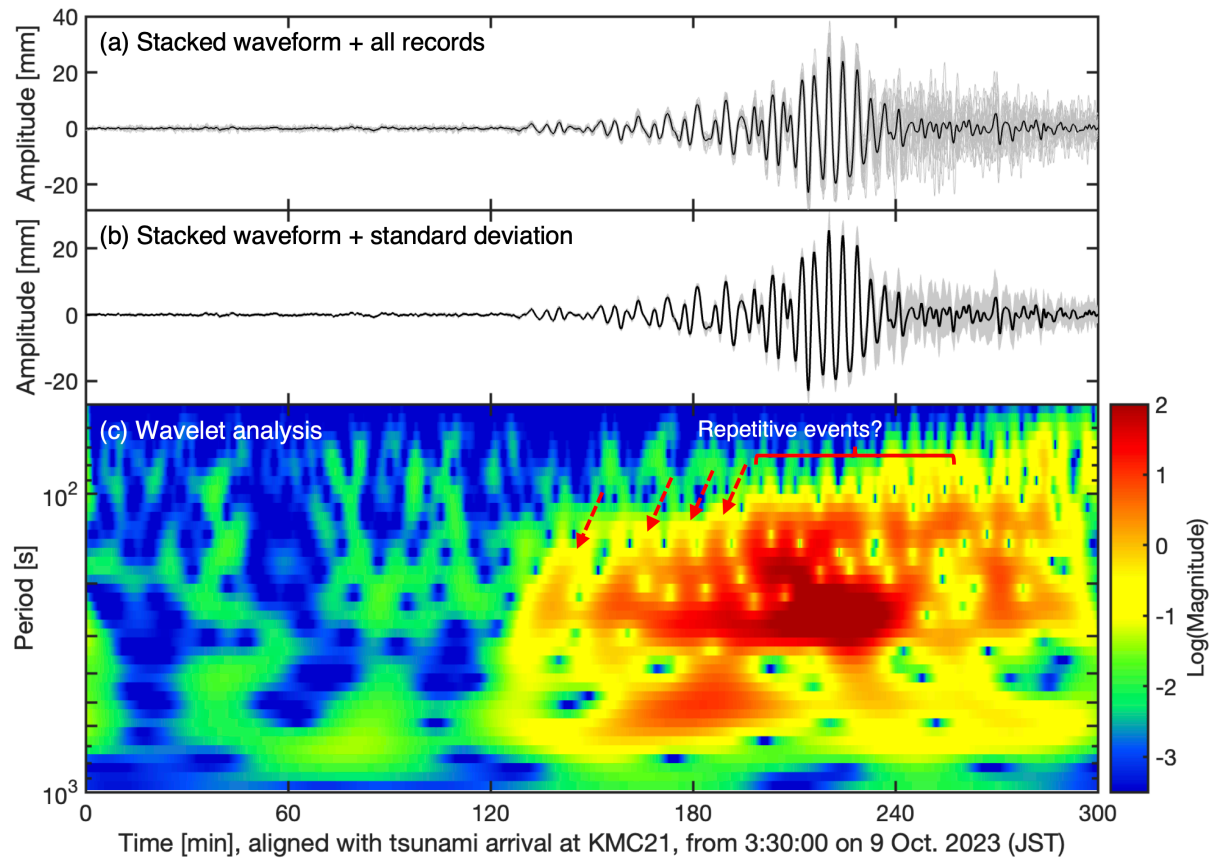
260   oceanic region.

Data availability

DONET data is available from NIED (National Research Institute for Earth Science and Disaster Resilience, 2019) (https://www.seafloor.bosai.go.jp/). We use bathymetric data of JTOPO30, which are available from the Japan Hydrographic Association (http://www.mirc.jha.jp/products/finished/JTOPO30/). Earthquake information is available from U. S. Geological Survey (USGS: https://earthquake.usgs.gov/earthquakes/search/, accessed on 19 October 2023).
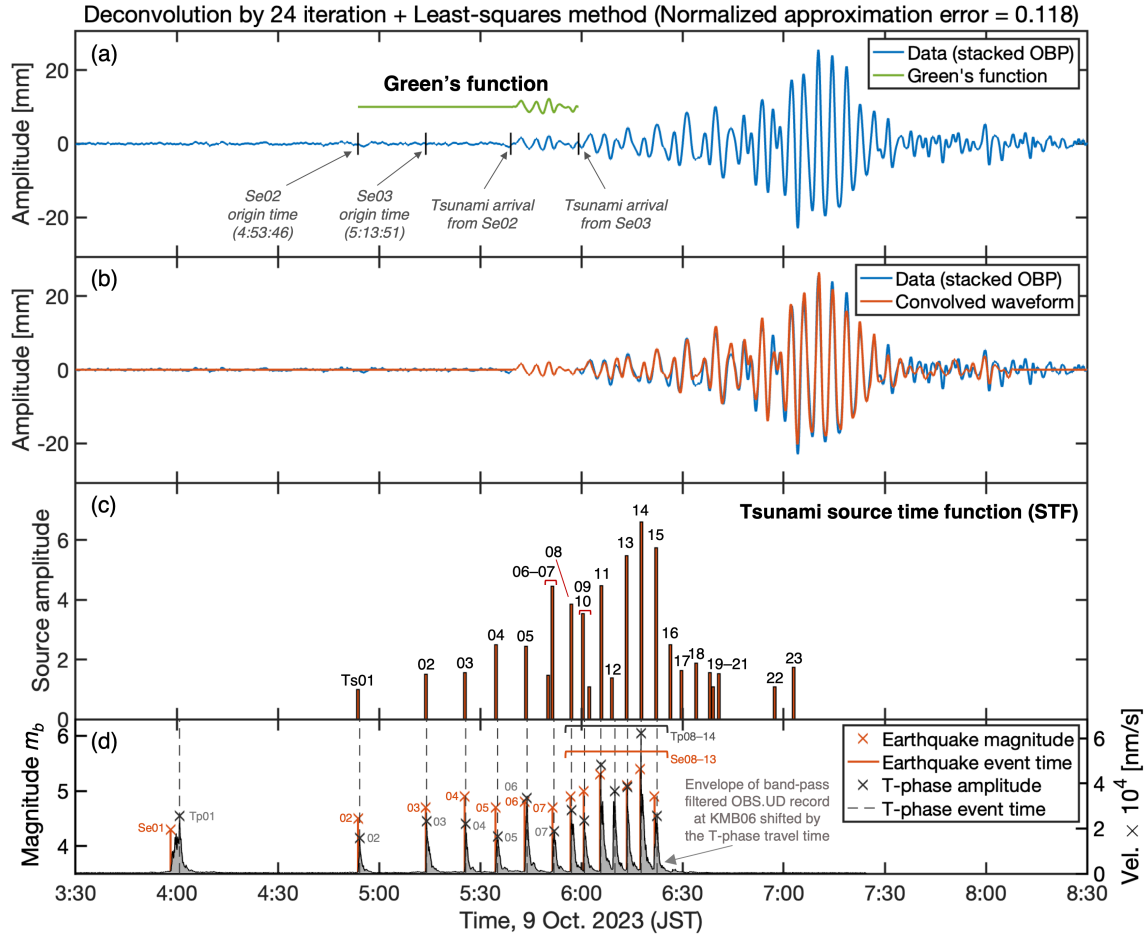
Figure 1. Maps of the study area. (**a**) Philippine Sea off southwestern Japan region. Red inverted triangles represent locations of tide gauges with the maximum tsunami heights reported by JMA. (**b**) Orange inverted triangles represent the DONET stations. (**c**) The region near Torishima Island. Black open and closed circles represent the locations of seismic events at depths of <20 km from 2 to 8 October 2023 (JST), and on 9 October 2023, respectively, reported in the USGS earthquake catalog. Red triangles represent active volcanoes documented in (Hydrographic and Oceanographic Department, Japan Coast Guard, 2006).
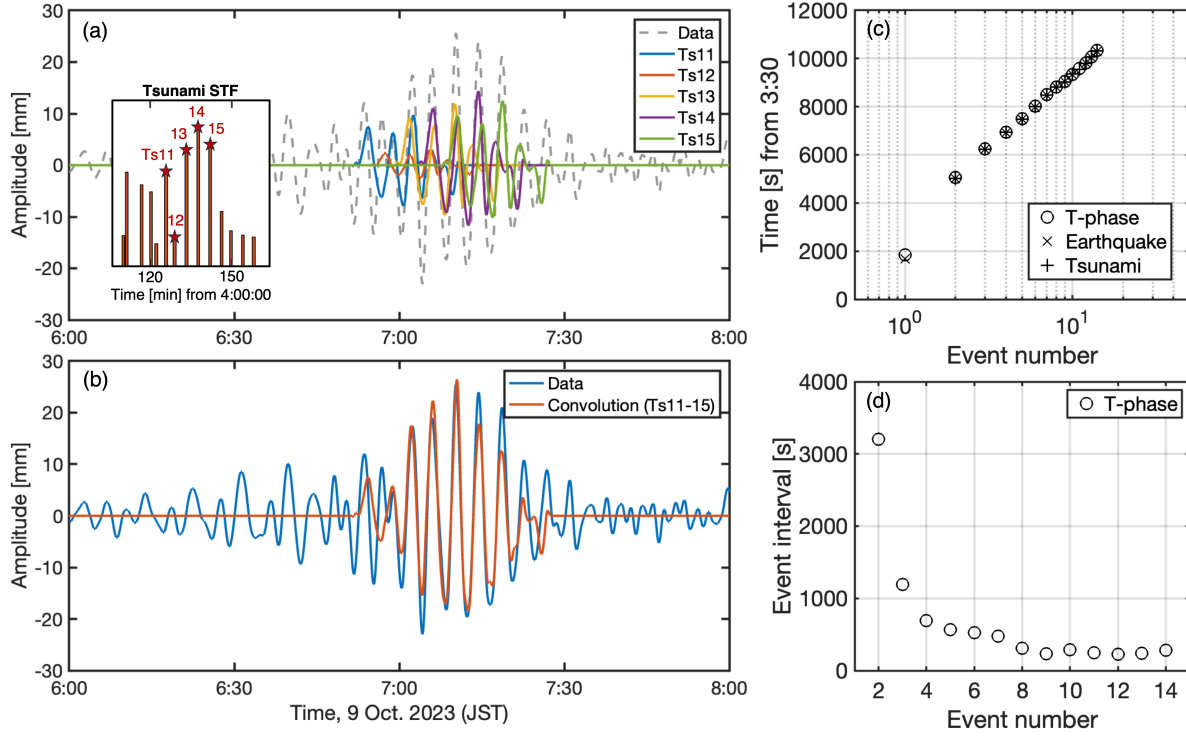
281

Figure 2. OBP data of DONET after 3:30:00 on 9 October 2023 (JST). (**a**) Data after removing the tidal trend by polynomial approximation, and (**b**) after the tidal-trend removal and the band-pass filter (0.00125–0.02 Hz), in the frequency range where tsunami signals are dominant. The amplitudes are in unit of water wave height [mm] converted from pressure, using 1.0 [Pa] = 0.102 [mmH$_2$O].

287

288

Figure 3. Waveform stacking of 16 OBP tsunami data from DONET1 (Table S2). (**a**) The stacked tsunami waveform (thick black line) and the 16 waveforms used for the stacking (thin gray lines). (**b**) The stacked waveform (thick black line) ± the standard deviation (shaded by gray). (**c**) Wavelet analysis for the stacked waveform by the continuous wavelet transformation in MATLAB (Lilly, 2017). Red arrows and a curly blacked indicate multiple bands of amplitude peaks of tsunami wave trains.

Figure 4. The tsunami STF by the iterative deconvolution (24 times) and the least-squares method. (**a**) The Green's function (green line) obtained from the stacked OBP tsunami waveform (blue line). (**b**) The convolved tsunami waveform (red line) compared with the stacked waveform. (**c**) Tsunami STF, composed of 23 source events (Ts01–Ts23; Table S3). The source amplitudes are relative to that of Ts01. (**d**) The temporal history of the seismic events (Se01–13) and the T-phase events (Tp01–14), and the envelope of the up-down component of OBS at KMB06, shifted backward in time by the T-phase travel time at 1.5 km/s (5.48 [min]) (gray shade).

Figure 5. Tsunami waves of the later events. (**a**) The waveforms due to each event of Ts11–15, shown in the inset panel. (**b**) The convolved waveform with Ts11–15 (orange line) and the stacked waveform (blue line). (**c–d**) The relationship between (**c**) the event number and timing, for source events EV01–14, determined by tsunamis, seismic body-waves, and T-phases, and (**d**) between the event number and the interval times of the T-phase events.

311 **References**

312 Abe, K. (1981). Physical size of tsunamigenic earthquakes of the northwestern Pacific. *Physics of the Earth*

313 *and Planetary Interiors*, *27*(3), 194–205. https://doi.org/10.1016/0031-9201(81)90016-9

314 Ewing, M., Tolstoy, I., & Frank Press. (1950). Proposed use of the T phase in tsunami warning systems.

315 *Bulletin of the Seismological Society of America*, *40*(1), 53–58.

316 https://doi.org/10.1785/BSSA0400010053

317 Fukao, Y., Sandanbata, O., Sugioka, H., Ito, A., Shiobara, H., Watada, S., & Satake, K. (2018). Mechanism of

318 the 2015 volcanic tsunami earthquake near Torishima, Japan. *Science Advances*, *4*(4), eaao0219.

319 https://doi.org/10.1126/sciadv.aao0219

320 Grilli, S. T., Tappin, D. R., Carey, S., Watt, S. F. L., Ward, S. N., Grilli, A. R., et al. (2019). Modelling of the

321 tsunami from the December 22, 2018 lateral collapse of Anak Krakatau volcano in the Sunda Straits,

322 Indonesia. *Scientific Reports*, *9*(1), 11946. https://doi.org/10.1038/s41598-019-48327-6

323 Hydrographic and Oceanographic Department, Japan Coast Guard. (2006). Database of the Maritime and

324 Submarine Volcanoes in Japan. Retrieved October 14, 2023, from

325 https://www1.kaiho.mlit.go.jp/kaiikiDB/list-2.htm

326 Igarashi, G. (2000). A geodetic sign of the critical point of stress‐strain state at a plate boundary. *Geophysical*

327 *Research Letters*, *27*(13), 1973–1976. https://doi.org/10.1029/1999gl005443

328 Japan Meteorological Agency. (2023, October 9). Report on Earthquake near Torishima Island around 5:25 on

329 October 9, 2023 (2nd report) (in Japanese). Retrieved October 19, 2023, from

330 https://www.jma.go.jp/jma/press/2310/09b/202310091100.html

331 Kanamori, H. (1972). Mechanism of tsunami earthquakes. *Physics of the Earth and Planetary Interiors*, *6*(5),

332 346–359. https://doi.org/10.1016/0031-9201(72)90058-1

333 Kanamori, H., Ekström, G., Dziewonski, A., Barker, J. S., & Sipkin, S. A. (1993). Seismic radiation by magma

334 injection: An anomalous seismic event near Tori Shima, Japan. *Journal of Geophysical Research*,

335 *98*(B4), 6511–6522. https://doi.org/10.1029/92jb02867

336   Kikuchi, B. Y. M., & Kanamori, H. (1982). Inversion of complex body waves. *Bulletin of the Selsmologmal*

337   *Socmty of America*, *72*(2), 491–506. x

338   Kodaira, S., Sato, T., Takahashi, N., Ito, A., Tamura, Y., Tatsumi, Y., & Kaneda, Y. (2007). Seismological

339   evidence for variable growth of crust along the Izu intraoceanic arc. *Journal of Geophysical Research*,

340   *112*(B5), B05104. https://doi.org/10.1029/2006jb004593

341   Kubota, T., Saito, T., & Nishida, K. (2022). Global fast-traveling tsunamis driven by atmospheric Lamb waves

342   on the 2022 Tonga eruption. *Science*, *377*(6601), 91–94. https://doi.org/10.1126/science.abo4364

343   Lilly, J. M. (2017). Element analysis: a wavelet-based method for analysing time-localized events in noisy

344   time series. *Proceedings. Mathematical, Physical, and Engineering Sciences / the Royal Society*,

345   *473*(2200), 20160776. https://doi.org/10.1098/rspa.2016.0776

346   Maeno, F., Imamura, F., & Taniguchi, H. (2006). Numerical simulation of tsunamis generated by caldera

347   collapse during the 7.3 ka Kikai eruption, Kyushu, Japan. *Earth, Planets and Space*, *58*(8), 1013–

348   1024. https://doi.org/10.1186/BF03352606

349   Matsumoto, H., Haralabus, G., Zampolli, M., & Özel, N. M. (2016). T‐phase and tsunami pressure

350   waveforms recorded by near‐source IMS water‐column hydrophone triplets during the 2015 Chile

351   earthquake. *Geophysical Research Letters*, *43*(24). https://doi.org/10.1002/2016gl071425

352   Michon, L., Villeneuve, N., Catry, T., & Merle, O. (2009). How summit calderas collapse on basaltic

353   volcanoes: New insights from the April 2007 caldera collapse of Piton de la Fournaise volcano.

354   *Journal of Volcanology and Geothermal Research*, *184*(1), 138–151.

355   https://doi.org/10.1016/j.jvolgeores.2008.11.003

356   Mulia, I. E., Watada, S., Ho, T.-C., Satake, K., Wang, Y., & Aditiya, A. (2020). Simulation of the 2018

357   tsunami due to the flank failure of anak krakatau volcano and implication for future observing

358   systems. *Geophysical Research Letters*, *47*(14), e2020GL087334.

359   https://doi.org/10.1029/2020gl087334

360   National Research Institute for Earth Science and Disaster Resilience. (2019). NIED DONET [Data set].

361   National Research Institute for Earth Science and Disaster Resilience.

362   https://doi.org/10.17598/NIED.0008

363 Okal, E. A. (2003). T Waves from the 1998 Papua New Guinea Earthquake and its Aftershocks: Timing the

364   Tsunamigenic Slump. In J.-P. Bardet, F. Imamura, C. E. Synolakis, E. A. Okal, & H. L. Davies (Eds.),

365   *Landslide Tsunamis: Recent Findings and Research Directions* (pp. 1843–1863). Basel: Birkhäuser

366   Basel. https://doi.org/10.1007/978-3-0348-7995-8_4

367 Okal, E. A. (2008). The generation of T waves by earthquakes. In R. Dmowska (Ed.), *Advances in Geophysics*

368   (Vol. 49, pp. 1–65). Elsevier. https://doi.org/10.1016/S0065-2687(07)49001-X

369 Paris, R. (2015). Source mechanisms of volcanic tsunamis. *Philosophical Transactions. Series A,*

370   *Mathematical, Physical, and Engineering Sciences*, *373*(2053). https://doi.org/10.1098/rsta.2014.0380

371 Purkis, S. J., Ward, S. N., Fitzpatrick, N. M., Garvin, J. B., Slayback, D., Cronin, S. J., et al. (2023). The 2022

372   Hunga-Tonga megatsunami: Near-field simulation of a once-in-a-century event. *Science Advances*,

373   *9*(15), eadf5493. https://doi.org/10.1126/sciadv.adf5493

374 Saito, T., & Furumura, T. (2009). Three-dimensional tsunami generation simulation due to sea-bottom

375   deformation and its interpretation based on the linear theory. *Geophysical Journal International*,

376   *178*(2), 877–888. https://doi.org/10.1111/j.1365-246X.2009.04206.x

377 Sandanbata, O., Watada, S., Satake, K., Kanamori, H., Rivera, L., & Zhan, Z. (2022). Sub‐decadal volcanic

378   tsunamis due to submarine trapdoor faulting at sumisu caldera in the Izu–Bonin arc. *Journal of*

379   *Geophysical Research, [Solid Earth]*, *127*(9), e2022JB024213. https://doi.org/10.1029/2022jb024213

380 Sandanbata, O., Watada, S., Satake, K., Kanamori, H., & Rivera, L. (2023). Two volcanic tsunami events

381   caused by trapdoor faulting at a submerged caldera near Curtis and Cheeseman islands in the

382   kermadec arc. *Geophysical Research Letters*, *50*(7), e2022GL101086.

383   https://doi.org/10.1029/2022gl101086

384 Satake, K., & Kanamori, H. (1991). Abnormal tsunamis caused by the June 13, 1984, Torishima, Japan,

385   earthquake. *Journal of Geophysical Research*, *96*(B12), 19933–19939.

386   https://doi.org/10.1029/91jb01903

387 Sugioka, H., Fukao, Y., Kanazawa, T., & Kanjo, K. (2000). Volcanic events associated with an enigmatic

388   submarine earthquake. *Geophysical Journal International*, *142*(2), 361–370.

389   https://doi.org/10.1046/j.1365-246x.2000.00153.x

390 Synolakis, C. E., Bardet, J.-P., Borrero, J. C., Davies, H. L., Okal, E. A., Silver, E. A., et al. (2002). The slump

391   origin of the 1998 Papua New Guinea Tsunami. *Proceedings of the Royal Society of London. Series A:*

392   *Mathematical, Physical and Engineering Sciences*, *458*(2020), 763–789.

393   https://doi.org/10.1098/rspa.2001.0915

394 Tanioka, Y., & Satake, K. (1996). Fault parameters of the 1896 Sanriku Tsunami Earthquake estimated from

395   Tsunami Numerical Modeling. *Geophysical Research Letters*, *23*(13), 1549–1552.

396   https://doi.org/10.1029/96GL01479

397 Tappin, D. R., Matsumoto, T., Watts, P., Satake, K., McMurtry, G. M., Matsuyama, M., et al. (1999).

398   Sediment slump likely caused 1998 Papua New Guinea tsunami. *Eos*, *80*(30), 329.

399   https://doi.org/10.1029/99eo00241

400 Yamada, M., Mori, J., & Matsushi, Y. (2016). Possible stick‐slip behavior before the Rausu landslide

401   inferred from repeating seismic events. *Geophysical Research Letters*, *43*(17), 9038–9044.

402   https://doi.org/10.1002/2016gl069288

403 Yamasato, H., Hamada, N., McCreery, C. S., Oliveira, F. J., Walker, D. A., & Talandier, J. (1993). T Waves

404   Associated with Submarine Volcanic Eruptions in the Marianas Observed by Ocean Bottom

405   Seismographs. *Journal of Physics of the Earth*, *41*(2), 57–74. https://doi.org/10.4294/jpe1952.41.57

406